Chemical Science

ROYAL SOCIETY OF CHEMISTRY

EDGE ARTICLE

View Article Online
View Journal | View Issue

Cite this: *Chem. Sci.*, 2025, **16**, 17812

All publication charges for this article have been paid for by the Royal Society of Chemistry

Cyclization-enhanced photoactivatable reversible room-temperature phosphorescence for efficient real-time light printing

Yonghui Sun, *[a] Yuqing Shu,[a] Li Zheng,[a] Yufei Song,[a] Baotong Huang,[b] Xiufang Xu,[b] Haohua Chen,*[a] Junbiao Chang[a] and Pengyang Xin *[a]

Received 7th July 2025
Accepted 24th August 2025

DOI: 10.1039/d5sc05008a

rsc.li/chemical-science

The construction of polymer-based photoactivated room-temperature phosphorescence systems remains a prominent research focus, yet the development of ultrafast activated systems under ambient conditions continues to pose a challenge. In this study, cyclized phenothiazine derivatives bearing diverse substituents are synthesized and incorporated into an amorphous polyvinyl alcohol (PVA) matrix, resulting in significantly enhanced dynamic photoactivation characteristics compared with those of their pristine monomeric counterparts. Under ambient conditions and 2 s irradiation, the lifetime and quantum yield of **C[4]PTZ-OH@PVA** increase by factors of 1.96 (from 11.8 to 23.1 ms) and 3.43 (from 8.62% to 29.53%), respectively, relative to those of **PTZ-OH@PVA**. Theoretical calculations and experimental data reveal the mechanism of ultrafast photoactivation: (1) the rigid cyclic architecture suppresses non-radiative decay and enhances the probability of intersystem crossing pathways; (2) the hydroxyl-substituted phenothiazine derivatives form an extensive hydrogen-bonding network with PVA, providing isolation from oxygen and moisture invasion while suppressing molecular vibrations. This synergistic effect enables rapid depletion of residual $^3O_2$ under irradiation, thereby accelerating the photoactivation of **C[4]PTZ-OH@PVA**. Notably, various patterns are printed on the films within 2 s, and then quickly erased after annealing. This study proposes a novel cyclization-enhanced strategy for photoactivated room-temperature phosphorescence, offering valuable guidance for the development of high-performance light-responsive materials.

1 Introduction

Organic room-temperature phosphorescence (RTP), renowned for its abundant triplet excitons and long luminescence lifetimes ranging from microseconds to hours, has found extensive applications in high-contrast bioimaging, anti-counterfeiting, and information encryption.[1] Compared with inorganic systems that involve high fabrication costs and non-negligible metal toxicity, polymer-based organic RTP materials typically employ cost-effective polymers, such as polyvinyl alcohol (PVA) and polymethyl methacrylate (PMMA) as matrices through simple physical doping, achieving significant improvements in the emission color, phosphorescence lifetime, and quantum yields.[2] To further expand RTP applications, recent research has focused on developing phosphorescent materials with external stimulus-responsive characteristics, as their luminescence color, intensity, and lifetime can reversibly change in response to mechanical forces, temperature, light, or electric fields.[3] These high environmental sensitivities broaden their potential applications. Among such materials, photoactivated RTP materials have received particular attention owing to their critical roles in optical printing, 3D displays, and information storage.[4] Currently photoactivated RTP systems are primarily categorized into small organic molecules and polymer-based materials.[5] While the light-induced manipulation of intermolecular interactions enables dynamic RTP in small molecules, their phosphorescence often diminishes when the crystalline order is disrupted by mechanical forces. In contrast, polymer-based photoactivated RTP systems exhibit superior robustness.[6,7] In addition, PVA has emerged as the most prevalent matrix for achieving long-lived RTP owing to its robust hydrogen-bonding network.[8,9] However, most reported photoactivated materials require activation times exceeding 10 s (Table S1), which hinders the realization of real-time light-label printing under ambient conditions. Therefore, the development of ultrafast photoactivated polymer RTP systems remains an urgent need.

Notably, molecular cyclization serves as an effective strategy for reducing the singlet–triplet energy gap and enhancing the intersystem crossing (ISC) efficiency, which are both critical for

[a]*State Key Laboratory of Antiviral Drugs, Pingyuan Laboratory, NMPA Key Laboratory for Research and Evaluation of Innovative Drug, School of Chemistry and Chemical Engineering, Henan Normal University, 46 Jianshe Road, Xinxiang, 453007, China. E-mail: syonghui1994@163.com; chenhaohua@htu.edu.cn; pyxin27@163.com; Tel: +86 373 3328652*

[b]*College of Chemistry State Key Laboratory of Elemento-Organic Chemistry Nankai University, Tianjin, 300071, China*

achieving RTP.[10] For example, the cyclization of carbazole derivatives significantly increases the phosphorescence lifetime from 1.45 ms in the monomeric form to 3.41 s in the cyclized form. This dramatic improvement arises from the significantly reduced singlet–triplet energy gap (0.04 eV) in the cyclized structure, which accelerates ISC rates.[11] Concurrently, the enhanced molecular rigidity suppresses non-radiative transitions. Therefore, the synergistic effect of cyclized molecules combined with PVA matrices is a promising strategy for realizing rapidly photoactivated RTP. Cyclized molecules promote the ISC efficiency by increasing the structural rigidity and conjugation. Meanwhile, the extensive hydrogen-bonding network of PVA anchors the molecules multi-directionally, effectively inhibiting non-radiative decay pathways.

Herein, we focused on exploring the photoactivated RTP of cyclized phenothiazine derivatives within polymer matrices. Cyclization not only enhances molecular conjugation strength and structural rigidity but also strengthens hydrogen-bonding interactions with polymer matrices in different spatial orientations, thereby creating greater potential for efficient RTP emission. Compared to phenothiazine monomers, the singlet–triplet energy gap of cyclized phenothiazine derivatives is minimized to 0.007 eV, providing a prerequisite for efficient intersystem crossing. Additionally, hydrogen bonding interactions between the hydrogen bond network of the PVA matrix and hydroxyl-terminated phenothiazine derivatives gradually strengthen with an increasing number of cyclic units. Rapid photoactivation is achieved within 2 s under light irradiation, with a significant enhancement in quantum yield from 8.62% (monomer) to 29.53% (cyclized tetramer) (Scheme 1). This molecular cyclization strategy for enhancing polymer-based photoactivation enables nearly delay-free optical printing, laying the foundation for applications in optical labeling.

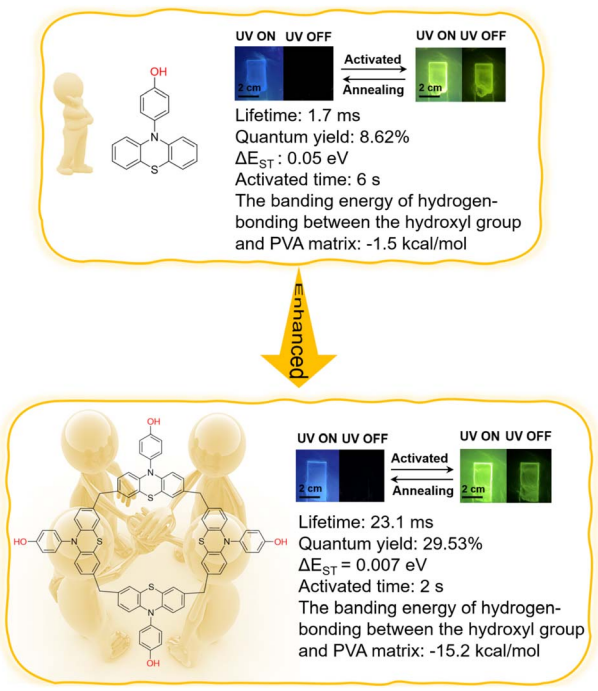

Scheme 1 The chemical structures of the monomer PTZ-OH and the cyclic tetramer C[4]PTZ-OH. In the PVA matrix, C[4]PTZ-OH exhibits superior optical properties compared to PTZ-OH.

2 Results and discussion

2.1 Synthesis and characterization of phenothiazine derivatives

Phenothiazine, a structural unit with an efficient singlet–triplet state communication, has been extensively studied for the construction of photoactivated RTP systems. By modifying the functional groups (–OCH_3, –OH, –$OCH_2CH{=}CH_2$) on the phenyl substituents and varying the number of cyclic units (n = 3, 4), we successfully synthesized three phenothiazine monomers (**PTZ-OCH_3**, **PTZ-OH**, and **PTZ-Pe**) and four cyclized phenothiazine derivatives (**C[3]PTZ-OCH_3**, **C[3]PTZ-OH**, **C[3]PTZ-Pe**, and **C[4]PTZ-OH**) in high yields. The detailed synthetic procedures are outlined in Scheme S1, and the structures of all compounds were comprehensively characterized by NMR spectroscopy (^{1}H, ^{13}C) and MALDI-TOF analysis (Fig. S1–S18).

Single crystals of **C[3]PTZ-OCH_3**, **C[3]PTZ-OH**, and **C[3]PTZ-Pe**, suitable for crystallography were obtained *via* slow diffusion: hexane/ethyl acetate for **C[3]PTZ-OH** and hexane/deuterated chloroform for **C[3]PTZ-OCH_3** and **C[3]PTZ-Pe**. All three compounds were found to adopt partial-cone conformations. The single-crystal data for these compounds are summarized in Table S2. Notably, **C[3]PTZ-OCH_3** crystallized in two distinct topological structures, exhibiting both aryl-substituted quasi-axial and quasi-equatorial conformations, which are stabilized by intermolecular C–H···π interactions (Fig. 1b). Compared with **C[3]PTZ-OH**, the longer aryl substituents in **C[3]PTZ-OCH_3** and **C[3]PTZ-Pe** suppress the flipping of the phenothiazine units, leading to more ordered molecular packing and a higher crystalline density in the solid state (Fig. S19), indicating their potential for phosphorescent emission in the solid state.

2.2 Photophysical properties of phenothiazine derivatives in the solution and solid state

First, the photophysical properties of the phenothiazine derivatives in the solution state were investigated. As shown in Fig. S20a, all compounds exhibited vibrational structures in the range of 230–350 nm, attributed to the n–π* and π–π* transitions of the phenothiazine unit. The absorbance of **C[4]PTZ-OH** increased significantly and displayed more pronounced vibrational features than those of **C[3]PTZ-OH** and **PTZ-OH**, likely owing to the combined effect of multiple phenothiazine units. In contrast, the absorbance of **PTZ-Pe** was stronger than that of **C[3]PTZ-Pe**, possibly originating from the hypochromic effect induced by the conjugated structure of the alkene moiety. **PTZ-OH**, **PTZ-Pe**, **C[3]PTZ-OH**, and **C[3]PTZ-Pe** exhibited fluorescence emission at 435 nm, indicating similar excited-state energy levels (Fig. S20b). For **PTZ-OCH_3**, the fluorescence emission peak appeared at 398 nm. Upon cyclization, this peak red-shifted to 409 nm because of the enhanced conjugation system. In contrast, **C[4]PTZ-OH** displayed a red-shifted

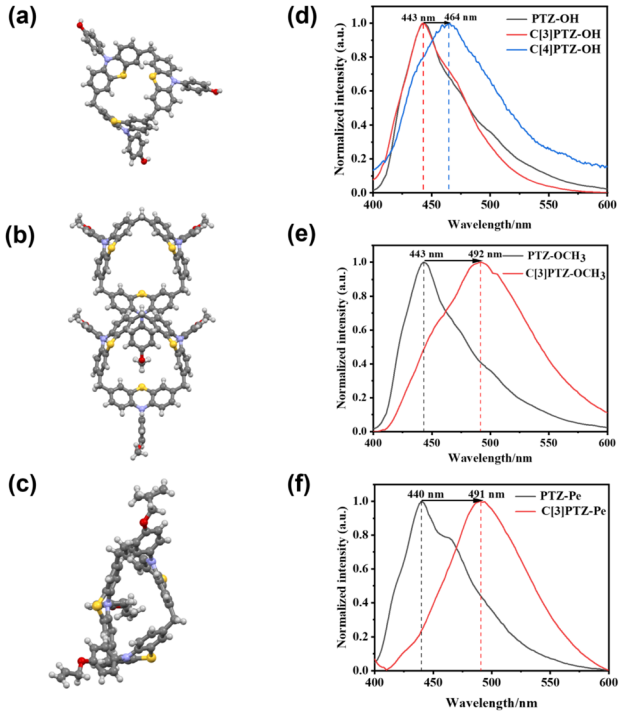

Fig. 1 Crystal structures of (a) **C[3]PTZ-OH** (deposition numbers 2449581), (b) **C[3]PTZ-OCH$_3$** (deposition numbers 2449557), and (c) **C[3]PTZ-Pe** (deposition numbers 2449607). Photoluminescence spectra in the solid state at 298 K of (d) **PTZ-OH**, **C[3]PTZ-OH**, and **C[4]PTZ-OH**; (e) **PTZ-OCH$_3$** and **C[3]PTZ-OCH$_3$**; and (f) **PTZ-Pe** and **C[3]PTZ-Pe**.

maximum emission wavelength of 454 nm, which was attributed to its extended conjugated structure.

Variable-temperature spectroscopic experiments were conducted to further investigate the luminescence properties of the compounds in solution under monomeric conditions (Fig. S21–S27). Steady-state spectra at 77 K revealed that all compounds exhibited fluorescence emission in the range of 400–450 nm and dual phosphorescence emission in the range of 475–600 nm in THF glass. The cyclized derivatives demonstrated a significantly higher triplet–state contribution than the phenothiazine monomer, indicating that cyclization promotes ISC. As the temperature gradually increased to 297 K, the phosphorescence emissions weakened and transitioned to fluorescence emissions in solution. Time-delayed spectra further confirmed the phosphorescent properties of the 475–600 nm bands. At a delay time of 100 μs, the fluorescence peaks disappeared, whereas the phosphorescence peaks gradually diminished with increasing temperature. Concurrently, the lifetime decay curves exhibited rapid decay, suggesting that molecular vibrations in solution induce substantial non-radiative dissipation. Notably, although cyclization facilitates triplet exciton accumulation, it also accelerates radiative transitions, resulting in longer phosphorescence lifetimes for the phenothiazine monomer derivatives than for their cyclized counterparts at 77 K. Subsequently, we investigated the photophysical properties of the derivatives in the solid state. As shown in Fig. 1d–f, steady-state photoluminescence spectra revealed that the cyclized derivatives **C[3]PTZ-OCH$_3$** and **C[3]PTZ-Pe** exhibited a red shift of approximately 50 nm in their photoluminescence compared with those of the monomers, suggesting potential phosphorescence emission in the solid state. The time-delayed spectra and lifetime decay curves further confirmed their phosphorescent properties in the amorphous state, although their lifetimes were only on the microsecond timescale (Fig. S28). In contrast, **PTZ-OH** and **C[3]PTZ-OH** showed no significant changes in their photoluminescence spectra, whereas **C[4]PTZ-OH** displayed a red shift of 21 nm relative to these derivatives, with the fluorescence emission centered at 464 nm.

2.3 Photophysical properties of phenothiazine derivatives in the films

Owing to the rigid structure of polymers and convenient doping strategies, polymer-based doping systems have become one of the most widely adopted approaches for achieving RTP. To further enhance the RTP performance of the phenothiazine derivatives, we conducted polymer doping experiments. Using PVA as the host matrix, the derivatives were physically blended with PVA at a doping concentration of 2 mg mL^{-1}, followed by casting and drying on glass slides to obtain polymer films (optimization of the doping concentration is discussed in SI, Fig. S29a and S29b). The average thickness of the films represented by **C[3]PTZ-OH@PVA** is 9.856 μm (Fig. S29c). As shown in Fig. 2a–c, **PTZ-OH@PVA**, **C[3]PTZ-OH@PVA**, and **C[4]PTZ-OH@PVA** exhibited emission profiles similar to those observed in the 77 K solution, suggesting that the phosphors were monodispersed within the PVA matrix. The overlap of delayed and steady-state spectra confirmed the phosphorescent properties of **PTZ-OH@PVA**, **C[3]PTZ-OH@PVA**, and **C[4]PTZ-OH@PVA** in the range of 500–550 nm, with corresponding phosphorescence lifetimes of 1.7, 2.9, and 6.1 ms, respectively. Previous studies have reported that light irradiation can deplete triplet oxygen in polymer films, thereby mitigating triplet exciton quenching. Remarkably, upon several seconds of UV exposure, the films emitted an intense yellow luminescence, which persisted as a visible yellow afterglow after the UV lamp was turned off (Video S1). We characterized the photoactivated RTP properties of all polymer films. The steady-state spectra revealed that the phosphorescence emission peaks gradually intensified and stabilized within 12 s of irradiation (Fig. 2d, e, and S30). Lifetime decay curves demonstrated that the phosphorescence lifetimes of **PTZ-OH@PVA**, **C[3]PTZ-OH@PVA**, and **C[4]PTZ-OH@PVA** increased to 11.8, 19, and 23.1 ms, respectively. Corresponding phosphorescence quantum yields rose from 3.53% to 8.62%, 8.04% to 27.16%, and 20.88% to 29.53% (Fig. 2f–i and S31–S33). The superior RTP performance of **C[4]PTZ-OH@PVA** suggests that hydroxyl-terminated phenothiazine derivatives formed stronger hydrogen-bonding interactions with PVA, which more effectively immobilized the phosphorescent units and enhanced their RTP efficiency. As shown in Fig. S34, the hydrogen–bonding energy within the doping system increases with the number of hydroxyl groups on the

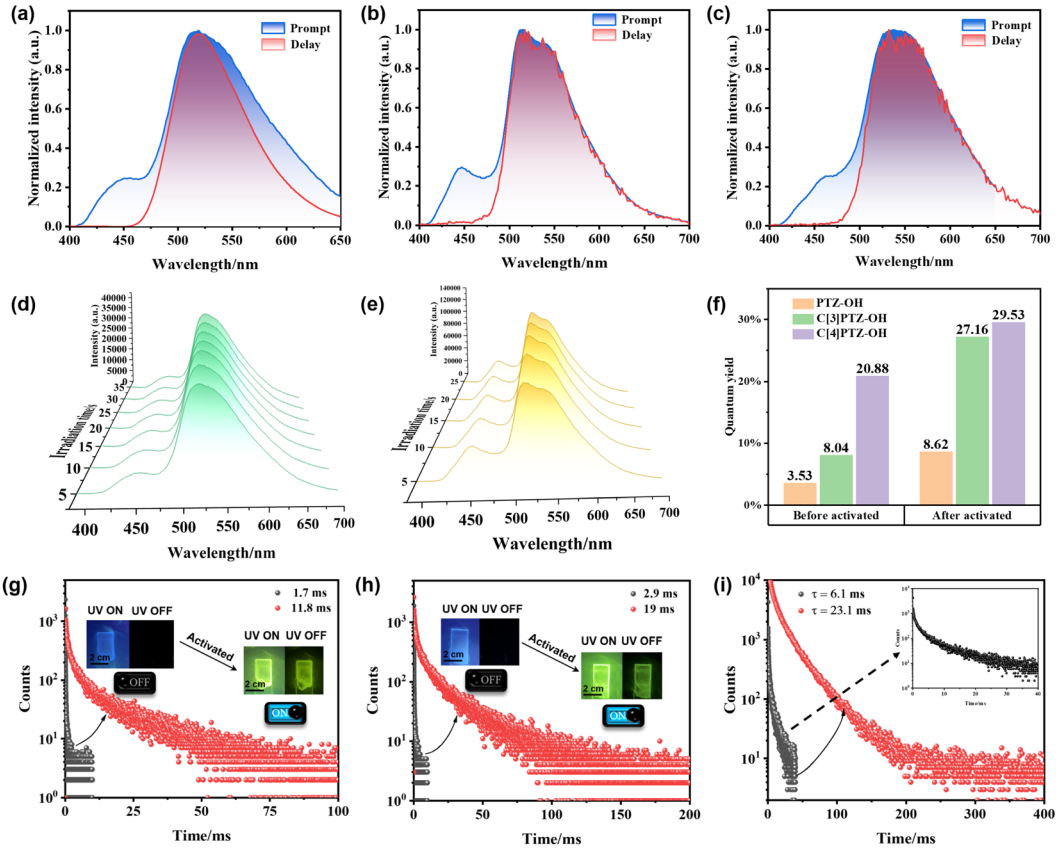

Fig. 2 Steady-state and delayed photoluminescence spectra (delay = 100 μs) of (a) PTZ-OH@PVA, (b) C[3]PTZ-OH@PVA, and (c) C[4]PTZ-OH@PVA. Changes in the emission spectra of (d) PTZ-OH@PVA and (e) C[3]PTZ-OH@PVA under UV irradiation at 365 nm (0.02 mW cm^{-2}). (f) Quantum yields of PTZ-OH@PVA, C[3]PTZ-OH@PVA, and C[4]PTZ-OH@PVA before and after photoactivation. Lifetime decay curves before and after the photoactivation of (g) PTZ-OH@PVA, (h) C[3]PTZ-OH@PVA, and (i) C[4]PTZ-OH@PVA. Inset: the photographs of PTZ-OH@PVA and C[3]PTZ-OH@PVA before and after photoactivation with a UV lamp (365 nm), followed by lamp shut down.

phenothiazine derivatives. Consequently, under identical irradiation conditions, **C[4]PTZ-OH@PVA** exhibited the fastest phosphorescence activation, longest phosphorescence lifetime, and highest quantum yield.

The photophysical properties of **PTZ-OCH_3@PVA** and **C[3]PTZ-OCH_3@PVA** are presented in SI. As shown in Fig. S35–S38, the phosphorescence of **PTZ-OCH_3@PVA** and **C[3]PTZ-OCH_3@PVA** gradually intensified under light irradiation. Both the steady-state and delayed spectra confirmed the phosphorescent emission and photoactivation processes. The lifetime decay curves revealed changes in lifetime before and after photoactivation, indicating that light irradiation activated the radiative transitions of the phosphorescent groups in the films. The corresponding phosphorescence quantum yields increase from 1.36% to 3.26% and 3.95% to 7.24%, respectively. Notably, because of the weak hydrogen bonding interactions between the allyl groups and PVA matrix, **PTZ-Pe@PVA** and **C[3]PTZ-Pe@PVA** did not exhibit phosphorescent emission in the PVA films, and even after light irradiation, this phenomenon remained negligible. Therefore, we investigated the phosphorescence properties of **PTZ-Pe** and **C[3]PTZ-Pe** in PMMA, a matrix more rigid than PVA. As shown in Fig. 3a, after 1 min of light irradiation (0.02 mW cm^{-2}), the fluorescence peak of **C[3]PTZ-Pe@PMMA** at 448 nm gradually weakened and shifted into a phosphorescence emission centered at 503 nm, which is consistent with the phosphorescent emission of **C[3]PTZ-Pe** in solution. The CIE chromaticity diagram illustrates the color transition from blue fluorescence to yellow–green phosphorescence (Fig. 3b). The overlap of steady-state and delayed spectra further confirmed the phosphorescence of the 503 nm emission peak. After activation, its lifetime was measured as 100 μs *via* lifetime decay curve analysis, while the corresponding quantum yield increased from 3.38% (before activation) to 4.45% (after activation) (Fig. S39 and S40).

The steady-state spectrum of **PTZ-Pe@PMMA** revealed that fluorescence dominated the radiative transition mechanism prior to illumination. After irradiation, lifetime measurements at 525 nm demonstrated its phosphorescent properties with a lifetime of 170 μs and an increase in the quantum yield from 2.52% (before activation) to 4.19% (after activation) (Fig. S41 and S42). Notably, for **PTZ-OCH_3@PMMA**, **C[3]PTZ-OCH_3@PMMA**, **C[3]PTZ-OH@PMMA**, **C[4]PTZ-OH@PMMA** and **PTZ-OH@PMMA**, their phosphorescence peaks progressively weaken under light irradiation, which stands in stark contrast to their photophysical properties within the PVA matrix (Fig. S43). Fig. 3c presents the photoactivation kinetics. In

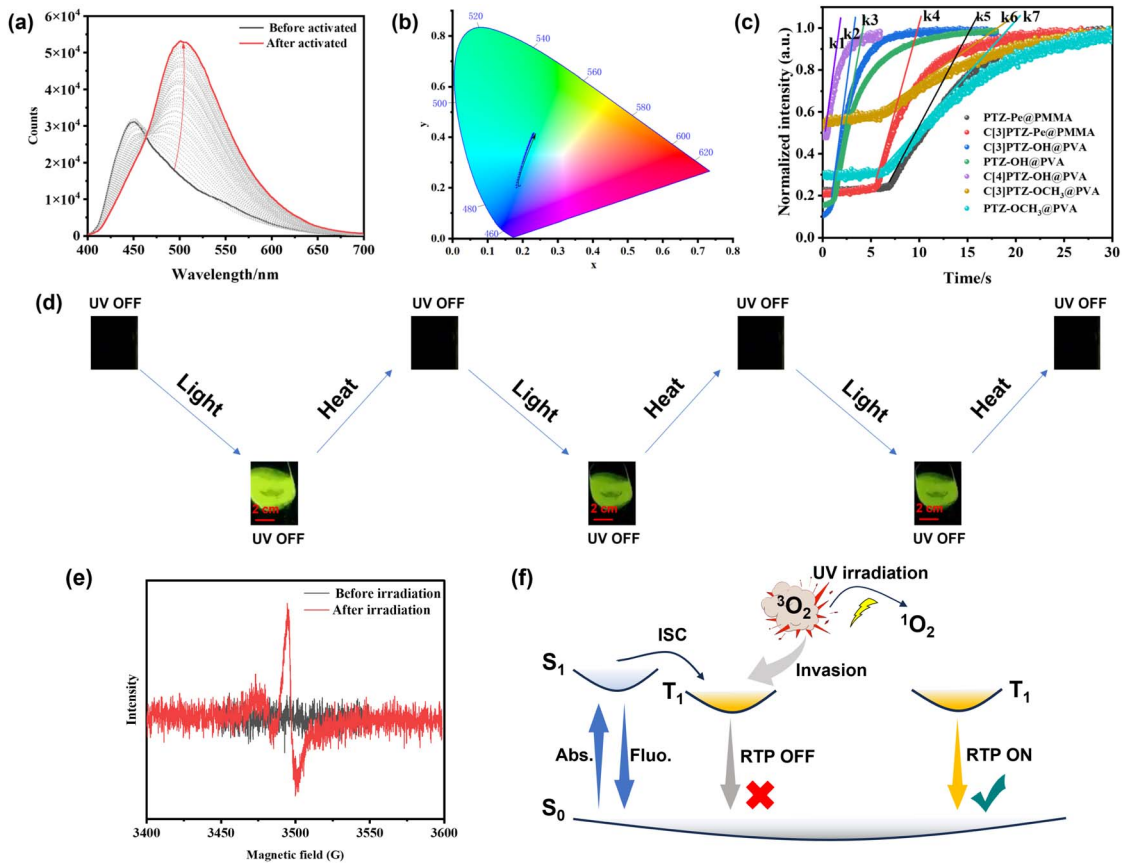

Fig. 3 (a) Steady-state photoluminescence spectra of **C[3]PTZ-Pe@PMMA** after irradiation for 0 (black line) to 60 s (red line). (b) CIE coordinates of **C[3]PTZ-Pe@PMMA** after irradiation for 0–60 s based on the CIE 1931 chromaticity diagram. (c) Normalized intensities of **PTZ-OH@PVA**, **C[3]PTZ-OH@PVA**, **C[4]PTZ-OH@PVA**, **PTZ-Pe@PMMA**, **C[3]PTZ-Pe@PMMA**, **PTZ-OCH$_3$@PVA**, and **C[3]PTZ-OCH$_3$@PVA** over time under continuous UV irradiation (365 nm, 150 W xenon light, excitation bandwidth = 2 nm, emission bandwidth = 3 nm). (d) Photographs of the photoactivated and thermally annealed afterglow of **C[3]PTZ-OH@PVA** under a UV lamp (365 nm). (e) Electron paramagnetic resonance spectra of **C[3]PTZ-OH@PVA** with 2,2,6,6-tetramethylpiperidine in the dark (black line) and after UV irradiation (red line). (f) Schematic diagram of the photoactivation mechanism.

comparison with the weak hydrogen-bonding interactions of **PTZ-Pe** and **C[3]PTZ-Pe** in PMMA, **PTZ-OH**, **C[3]PTZ-OH**, and **C[4]PTZ-OH** embedded in PVA exhibited significantly shorter photoactivation times, highlighting the critical role of the polyhydroxy hydrogen-bonding network. Furthermore, the cyclized derivatives demonstrated markedly faster photoactivation rates, indicating enhanced ISC rates and superior phosphorescence performance in these derivatives ($k_1 \approx k_2 > k_3 > k_4 > k_5$). Notably, **C[4]PTZ-OH@PVA** achieved near instantaneous illumination under light exposure, requiring only 4 s to reach the optimal photoactivated state, representing a substantial improvement over previously reported photoactivation systems. However, **PTZ-OCH$_3$@PVA** and **C[3]PTZ-OCH$_3$@PVA** displayed opposite trends, which may be attributed to the conformational changes in **C[3]PTZ-OCH$_3$** that promote faster non-radiative transitions. In addition, all films rapidly reverted to their original states upon thermal annealing at 60 °C for 20 s. Although the luminescence intensity gradually decreased over multiple cycles, the system maintained a relatively high phosphorescence emission efficiency (Fig. 3d and S44).

2.4 Mechanism

The consumption of oxygen within the film is a plausible mechanism underlying photoactivated RTP, as the presence of $^3O_2$ in the film constitutes the primary pathway for triplet exciton quenching. UV irradiation facilitates the depletion of $^3O_2$ by converting it into excited $^1O_2$. To verify $^1O_2$ trapping within the film, electron paramagnetic resonance (EPR) experiments were conducted. Two films containing 2,2,6,6-tetramethylpiperidine (TEMP) were prepared (TEMP ⊂ **C[3]PTZ-OH**@PVA), as TEMP reacts with $^1O_2$ to form the stable radical TEMPO, enabling the detection of $^1O_2$ generation. As shown in Fig. 3e, only the UV-irradiated film exhibited distinct EPR signals, whereas its non-irradiated counterpart showed no response. This observation confirms that oxygen depletion is a critical mechanism for activating phosphorescence. Fig. S45 visually demonstrates the dynamics of oxygen consumption and invasion in the film. After oxygen was depleted from the film, it continued to emit phosphorescence under UV irradiation for over 30 min in a nitrogen atmosphere. In contrast, when exposed to air, the film rapidly deactivated and returned to its

original state within 30 min owing to the re-invasion of oxygen. Furthermore, molecular cyclization played a crucial role in enhancing the phosphorescence emission of the phenothiazine derivatives. To shed light on the structure–property correlations between molecular architectures and excited-state energetics in phenothiazine derivatives, we conducted comprehensive density functional theory and time-dependent DFT calculations at the M062X-D3/def2-SVP level of theory. Fig. 4 shows the calculated singlet-triplet energy gaps (ΔE_{ST}), spin–orbit coupling (SOC) values, and frontier molecular orbital energy level distributions (HOMO and LUMO). In principle, a high SOC value (>0.3 cm^{-1}) is essential for achieving efficient ISC, and energy levels within the $E_{S1} \pm 0.3$ eV window represent potential transition channels from S_1 to T_n. More was found through comparison of the energy levels of monomers (**PTZ-OH**, **PTZ-OCH$_3$**, and **PTZ-Pe**) and cyclized trimers (**C[3]PTZ-OH**, **C[3]PTZ-OCH$_3$**, **C[3]PTZ-Pe**) that the number of orbitals with an energy gap (ΔE_{ST}) between S_1 and T_n within the range of 0.3 eV is increased in the latter, which was favorable for the ISC process. Such as, the monomers **PTZ-OH** and **PTZ-Pe** exhibit four possible ISC channels from S_1 to T_2, T_3, T_4 and T_5, with minimum ΔE_{ST} values of 0.05 and 0.06 eV, respectively (Fig. 4a and c, top panels; Table S3 and S4), while the corresponding cyclized trimer **C[3]PTZ-OH** exhibits seven effective ISC channels $S_1 \rightarrow T_4$ ($\Delta E_{ST} = 0.19$, SOC = 0.85 cm^{-1}), $S_1 \rightarrow T_5$ ($\Delta E_{ST} = 0.18$, SOC = 4.98 cm^{-1}), $S_1 \rightarrow T_6$ ($\Delta E_{ST} = 0.159$, SOC = 3.61 cm^{-1}), $S_1 \rightarrow T_7$ ($\Delta E_{ST} = 0.02$, SOC = 0.07 cm^{-1}), $S_1 \rightarrow T_8$ ($\Delta E_{ST} = 0.012$, SOC = 0.07 cm^{-1}), $S_1 \rightarrow T_9$ ($\Delta E_{ST} = 0.0116$, SOC = 0.05 cm^{-1}), and $S_1 \rightarrow T_{10}$ ($\Delta E_{ST} = 0.018$, SOC = 2.20 cm^{-1}) with the smallest ΔE_{ST} of 0.01 eV (Fig. 4a, bottom panel; Table S5). This clearly demonstrates that the cyclization significantly reduces the energy gaps and resolves the problem of insufficient single–triplet transition. Similarly, **C[3]PTZ-OCH$_3$** and **C[3]PTZ-Pe** present seven and eight effective ISC channels, with minimum ΔE_{ST} values of 0.007 ($S_1 \rightarrow T_8$) and 0.02 eV ($S_1 \rightarrow T_5$) respectively (Fig. 4b and c, bottom panels; Tables S6 and S7). Thus, **C[3]PTZ-OH**, **C[3]PTZ-OCH$_3$** and **C[3]PTZ-OH** are capable of generating more triplet excitons, thereby achieving superior inherent phosphorescences compared with those of their pristine monomeric counterparts. This observation is consistent with the experimental data. Notably, **C[4]PTZ-OH** demonstrates an energy gap of only 0.007 eV between S_1 and T_8 (Fig. S46 and Table S8), indicating that increasing the number of cyclization

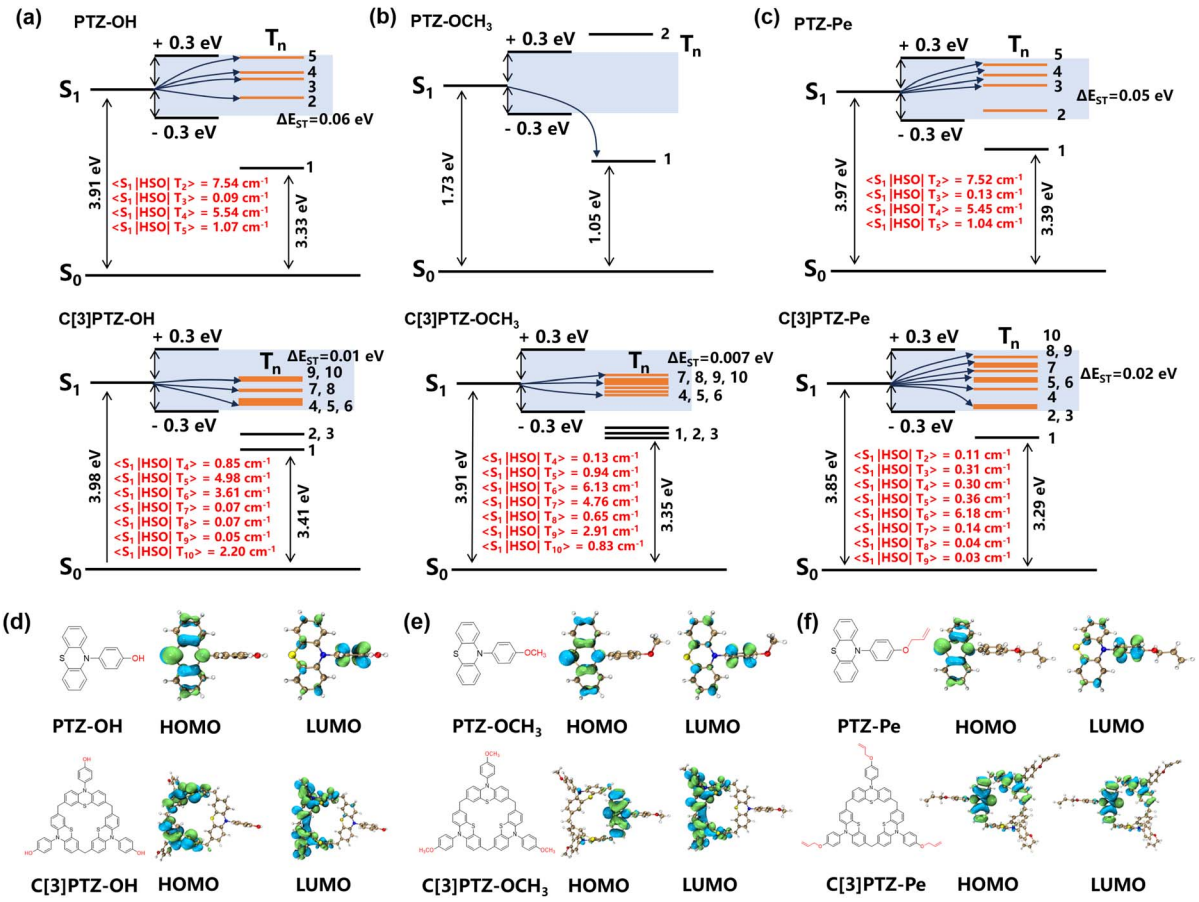

Fig. 4 Energy level diagrams and SOC values of (a) PTZ-OH, C[3]PTZ-OH, (b) PTZ-OCH$_3$, C[3]PTZ-OCH$_3$, and (c) PTZ-Pe, C[3]PTZ-Pe obtained from time-dependent density functional theory calculations. Triplet states available for efficient intersystem crossing are highlighted in orange. (d) Highest occupied and lowest unoccupied molecular orbital (HOMO and LUMO, respectively) topologies calculated *via* density functional theory for (d) PTZ-OH, C[3]PTZ-OH, (e) PTZ-OCH$_3$, C[3]PTZ-OCH$_3$, and (f) PTZ-Pe, and C[3]PTZ-Pe.

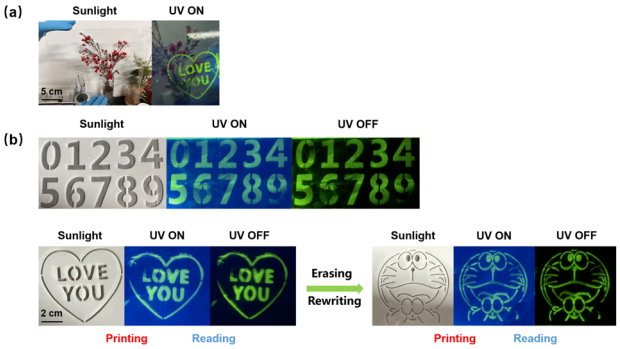

Fig. 5 (a) Schematic diagram of the high transparency of the thin film and high-brightness light-printed patterns under daylight. (b) The pattern of the leftmost photomask is printed onto the thin film through light exposure: luminescence under 365 nm UV irradiation (169 mW cm^{-2}) and afterglow following UV light deactivation.

units effectively reduces the ΔE_{ST} and improves the phosphorescence performance.

2.5 Application

Through drop-casting, large-area, highly transparent thin films can be prepared on glass substrates in a cost-effective and efficient manner. As shown in Fig. 5a, luminescent labels displaying "LOVE YOU" patterns can be contactless printed onto these films using only light irradiation. This process is completed within seconds with negligible delay, demonstrating its superior application potential in optical printing and luminescent labeling compared with those of previously reported systems. Furthermore, luminescent labeling can be repeatedly printed on film-coated glass substrates for over ten cycles, consistently maintaining a high contrast and clarity after rewriting. As illustrated in Fig. 5b, thermally annealed-erased films can be re-printed with various luminescent patterns, including "Doraemon," "LOVE YOU," and numerical characters ("0–9"), all of which exhibit persistent afterglow lasting several seconds following UV lamp deactivation. This simple and convenient approach to the on-demand writing of luminescent labels demonstrates strong potential as a next-generation alternative to conventional marking technologies.

3 Conclusions

In summary, we developed a cyclization-enhanced photoactivation strategy for polymer-based materials. These initially phosphorescence-silent films achieved a phosphorescence quantum yield of 29.53% and exhibited a visible afterglow to the naked eye after just a few seconds of light irradiation. EPR experiments confirmed that light-induced oxygen depletion within the films was critical for enabling phosphorescence emission. Theoretical calculations further revealed that cyclization not only rigidified the molecular structure and minimized the singlet–triplet energy gap, but also strengthened hydrogen-bonding interactions with the PVA matrix, thereby partially suppressing nonradiative decay. This strategy is expected to offer new insights into the development of delay-free optical printing and labeling technologies.

Author contributions

Y. S. conceived the idea and designed the research. Y. S. and L. Z. synthesized molecules together and performed all photophysical tests on the films. Y. S. conducted the application of light printing. Y. S., B. H. and X. X. carried out theoretical calculation. Y. S. and H. C. wrote the manuscript of this work. J. C. and P. X. provided constructive suggestions for results and helped revise the paper. All authors participated in the discussion.

Conflicts of interest

The authors declare no competing interest.

Data availability

Dataset: **https://figshare.com/s/b97527adc615f8523a36**.

The data supporting this article have been included as part of the SI. See DOI: **https://doi.org/10.1039/d5sc05008a**.

CCDC 2449557, 2449581 and 2449607 contain the supplementary crystallographic data for this paper.[11a–c]

Acknowledgements

We acknowledge funding from the National Natural Science Foundation of China (22271079, 821301032, and 22401088), Henan Province Science Foundation for Youths (252300420786), Research Project from Pingyuan Laboratory (2023PY-ZZ-0201), Special Project for Fundamental Research in the University of Henan Province (21ZX005), Central Plains Scholars and Scientists Studio Fund (2018002) and Henan Normal University Research Foundation for the Doctoral Program (QD2023058). We also acknowledge financial support from the Henan Key Laboratory of Organic Functional Molecules and Drug Innovation.

Notes and references

1 (*a*) W. Zhao, Z. He and B. Z. Tang, *Nat. Rev. Mater.*, 2020, **5**, 869; (*b*) X. K. Ma and Y. Liu, *Acc. Chem. Res.*, 2021, **54**, 3403–3414; (*c*) D. Guo, W. Wang, K. Zhang, J. Chen, Y. Wang, T. Wang, W. Hou, Z. Zhang, H. Huang, Z. Chi and Z. Yang, *Nat. Commun.*, 2024, **15**, 3598; (*d*) Y. Peng, X. Yao, X. Hu, B. Wu, X. Pei, Y. Yang, Z. Dong, Z. An, W. Huang and T. Cai, *Adv. Mater.*, 2024, **36**, 2406618; (*e*) Y. Wang, W. Ye, T. Cao, C. Wang, H. Meng, Z. Gao and C. Wang, *Chem. Eng. J.*, 2024, **481**, 148642; (*f*) L. Zhang, J. Li, Y. Zhang, W. Dai, Y. Zhang, X. Gao, M. Liu, H. Wu, X. Huang, Y. Lei and D. Ding, *Nat. Commun.*, 2025, **16**, 3970.

2 (*a*) Y. Zhang, Y. Su, H. Wu, Z. Wang, C. Wang, Y. Zheng, X. Zheng, L. Gao, Q. Zhou, Y. Yang, X. Chen, C. Yang and Y. Zhao, *J. Am. Chem. Soc.*, 2021, **143**, 13675; (*b*) X. Zheng, Q. Han, Q. Lin, C. Li, J. Jiang, Q. Guo, X. Ye, W. Z. Yuan,

Y. Liu and X. Tao, *Mater. Horiz.*, 2023, **10**, 197; (*c*) L. Zhou, J. Song, Z. He, Y. Liu, P. Jiang, T. Li and X. Ma, *Angew. Chem., Int. Ed.*, 2024, **63**, e202403773; (*d*) X. Li, W. Li, Z. Deng, X. Ou, F. Gao, S. He, X. Li, Z. Qiu, R. T. K. Kwok, J. Sun, D. L. Phillips, J. W. Y. Lam, Z. Guo and B. Z. Tang, *J. Am. Chem. Soc.*, 2025, **147**, 14198.

3 (*a*) Z. Q. Yao, J. Xu, B. Zou, Z. Hu, K. Wang, Y. J. Yuan, Y. P. Chen, R. Feng, J. B. Xiong, J. Hao and X. H. Bu, *Angew. Chem., Int. Ed.*, 2019, **58**, 5614; (*b*) Q. Huang, X. Mei, Z. Xie, D. Wu, S. Yang, W. Gong, Z. Chi, Z. Lin and Q. Ling, *J. Mater. Chem. C*, 2019, **7**, 2530; (*c*) X. Bi, Y. Shi, T. Peng, S. Yue, F. Wang, L. Zheng and Q. E. Cao, *Adv. Funct. Mater.*, 2021, **31**, 2101312; (*d*) L. Lu, K. Wang, H. Wu, A. Qin and B. Z. Tang, *Chem. Sci.*, 2021, **12**, 7058; (*e*) Y. Zhang, L. Gao, X. Zheng, Z. Wang, C. Yang, H. Tang, L. Qu, Y. Li and Y. Zhao, *Nat. Commun.*, 2021, **12**, 2297.

4 (*a*) M. Louis, H. Thomas, M. Gmelch, A. Haft, F. Fries and S. Reineke, *Adv. Mater.*, 2019, **31**, 1807887; (*b*) H. Li, H. Li, W. Wang, Y. Tao, S. Wang, Q. Yang, Y. Jiang, C. Zheng, W. Huang and R. Chen, *Angew. Chem., Int. Ed.*, 2020, **59**, 4756; (*c*) Y. Yang, J. Wang, D. Li, J. Yang, M. Fang and Z. Li, *Adv. Mater.*, 2021, **33**, 2104002; (*d*) H. Sun, S. Shen and L. Zhu, *ACS Mater. Lett.*, 2022, **4**, 1599; (*e*) C. Qian, Z. Ma, X. Fu, X. Zhang, Z. Li, H. Jin, M. Chen, H. Jiang, X. Jia and Z. Ma, *Adv. Mater.*, 2022, **34**, 2200544; (*f*) S. Xiong, Y. Xiong, D. Wang, Y. Pan, K. Chen, Z. Zhao, D. Wang and B. Z. Tang, *Adv. Mater.*, 2023, **35**, 2301874; (*g*) Y. Wang, A. Shao, J. Li, J. Wei, K. Wei, S. Liu, Y. Ma and Q. Zhao, *Angew. Chem., Int. Ed.*, 2024, **64**, e202416189; (*h*) B. L. Zhang, L. Miao, W. T. Song, J. J. Zhang, J. Chen, T. Wang, W. Q. Zhang, J. Ni and Z. Zhao, *Adv. Funct. Mater.*, 2024, **35**, 2415094; (*i*) G. Xie, N. Guo, X. Xue, Q. Yang, X. Liu, H. Li, H. Li, Y. Tao, R. Chen and W. Huang, *J. Am. Chem. Soc.*, 2024, **146**, 20449; (*j*) J. Zhou, B. Tian, Y. Zhai, M. Wang, S. Liu, J. Li, S. Li, T. D. James and Z. Chen, *Nat. Commun.*, 2024, **15**, 7198; (*k*) Q. Zhang, P. Hu, C. Han, Z. Mao, R. Chen, Z. Liang, W. Cai, L. Wang, Z. Yang, C. Zheng, C. Liu, G. Shi and B. Xu, *Adv. Opt. Mater.*, 2024, **12**, 2400642.

5 (*a*) L. Gu, H. Shi, M. Gu, K. Ling, H. Ma, S. Cai, L. Song, C. Ma, H. Li, G. Xing, X. Hang, J. Li, Y. Gao, W. Yao, Z. Shuai, Z. An, X. Liu and W. Huang, *Angew. Chem., Int. Ed.*, 2018, **57**, 8425; (*b*) M. Gu, H. Shi, K. Ling, A. Lv, K. Huang, M. Singh, H. Wang, L. Gu, W. Yao, Z. An, H. Ma and W. Huang, *Research*, 2020, 2020, DOI: **10.34133/2020/8183450**; (*c*) L. Yue, Q. Sun, Y. Zhang, Y. Wang, S. Cui, H. Zhang, S. Xue and W. Yang, *Chem. Eng. J.*, 2022, **433**, 134307; (*d*) Y. Gao, W. Ye, K. Qiu, X. Zheng, S. Yan, Z. Wang, Z. An, H. Shi and W. Huang, *Adv. Mater.*, 2023, **35**, 2306501.

6 (*a*) M. Gmelch, H. Thomas, F. Fries and S. Reineke, *Sci. Adv.*, 2019, **5**, eaau7310; (*b*) Y. Miao, F. Lin, D. Guo, J. Chen, K. Zhang, T. Wu, H. Huang, Z. Chi and Z. Yang, *Sci. Adv.*, 2024, **10**, eadk3354; (*c*) G. Yang, S. Hao, X. Deng, X. Song, B. Sun, M.-D. Li, W. J. Hyun and L. Dang, *Nat. Commun.*, 2024, **15**, 4674; (*d*) M. Zhang, X. Lan, M. Ding, C. Han, X. W. Liu, Z. Meng, Z. Q. Yu and Z. An, *Angew. Chem., Int. Ed.*, 2025, **64**, e202415250; (*e*) J. A. Li, L. Zhang, C. Wu, Z. Huang, S. Li, H. Zhang, Q. Yang, Z. Mao, S. Luo, C. Liu, G. Shi and B. Xu, *Angew. Chem., Int. Ed.*, 2023, **62**, e202217284.

7 (*a*) J. Huang, L. Qu, L. Gao, X. Wang, Q. Chen, Y. Wang, Y. Zhu, C. Li, Y. Li and C. Yang, *Macromolecules*, 2024, **57**, 5018; (*b*) B. Ding, X. Ma and H. Tian, *Acc. Mater. Res.*, 2023, **4**, 827; (*c*) Z. Guan, Z. Tang, J. Zeng, Y. Zheng, L. Ding, D. Chen, H. Li and X. Liu, *Adv. Sci.*, 2024, **11**, 2402632; (*d*) W.-W. Xu, Y. Chen, X. Xu and Y. Liu, *Small*, 2024, **20**, 2311087; (*e*) Z. Wu, Z. Xu, D. Wang, G. Deng, S. Lin, Z. Zhao, D. Wang, Y. Xiong and B. Z. Tang, *Adv. Funct. Mater.*, 2025, **35**, 2415285.

8 (*a*) Y. Sun, L. Jiang, L. Liu, Y. Chen, W.-W. Xu, J. Niu, Y. Qin, X. Xu and Y. Liu, *Adv. Opt. Mater.*, 2023, **11**, 2300326; (*b*) S. Li, Z.-Y. Zhang, J.-F. Lv, L. Li, J. Li and C. Li, *J. Mater. Chem. A*, 2023, **11**, 4957.

9 H. Zhu, I. Badía-Domínguez, B. Shi, Q. Li, P. Wei, H. Xing, M. C. R. Delgado and F. Huang, *J. Am. Chem. Soc.*, 2021, **143**, 2164.

10 Y. Wang, J. Yang, M. Fang, Y. Gong, J. Ren, L. Tu, B.-Z. Tang and Z. Li, *Adv. Funct. Mater.*, 2021, **31**, 2101719.

11 (*a*) Y. Sun, Y. Shu, L. Zheng, Y. Song, B. Huang, X. Xu, H. Chen, J. Chang and P. Xin, CCDC 2449557: Experimental Crystal Structure Determination, 2025, DOI: **10.5517/ccdc.csd.cc2n6yzt**; (*b*) Y. Sun, Y. Shu, L. Zheng, Y. Song, B. Huang, X. Xu, H. Chen, J. Chang and P. Xin, CCDC 2449581: Experimental Crystal Structure Determination, 2025, DOI: **10.5517/ccdc.csd.cc2n6zrm**; (*c*) Y. Sun, Y. Shu, L. Zheng, Y. Song, B. Huang, X. Xu, H. Chen, J. Chang and P. Xin, CCDC 2449607: Experimental Crystal Structure Determination, 2025, DOI: **10.5517/ccdc.csd.cc2n70lj**.